Available online at www.CivileJournal.org

Civil Engineering Journal

(E-ISSN: 2476-3055; ISSN: 2676-6957)

Vol. 11, No. 12, December, 2025

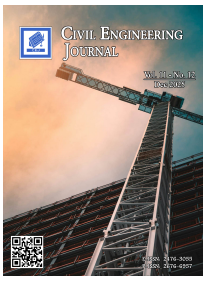

Advanced Retrofitting Solutions for RC Slabs: CFRP, ECC, and Steel Plate Comparison

Fatma M. Eid [1], Ahmed E. Sedawy [2*], Islam Ali Mahmoud [3]

[1] *Department of Civil Engineering, Menoufia University, Shibin El Kom, Egypt.*

[2] *Department of Civil Engineering, Misr Higher Institute for Engineering and Technology, Mansoura, Egypt.*

[3] *Department of Civil Engineering, Delta Higher Institute for Engineering & Technology, Mansoura, Egypt.*

Received 14 September 2025; Revised 19 November 2025; Accepted 25 November 2025; Published 01 December 2025

Abstract

Retrofitting reinforced concrete (RC) slabs is crucial for enhancing their flexural strength, ductility, and durability, particularly in aging or seismically deficient structures. This study aims to evaluate and compare the effectiveness of three retrofitting techniques: steel plate bonding, carbon fiber reinforced polymer (CFRP) sheets, and engineered cementitious composites (ECC) with expanded steel mesh in improving the structural behavior of RC slabs. The research integrates both experimental testing and numerical analysis using ABAQUS finite element modeling to assess load–deflection behavior, failure mechanisms, and strength enhancement. The findings revealed that the use of CFRP sheets and ECC with expanded mesh significantly improved the slabs' structural performance, increasing ultimate load capacity by up to 58% and ductility by more than 40% compared to the control specimens. Conversely, steel plate retrofitting showed inferior performance due to inadequate interfacial bonding. The numerical results exhibited strong agreement with the experimental data, with an average FEM-to-test ratio of 1.04. The study highlights the superior efficiency of CFRP and ECC techniques in strengthening RC slabs, offering enhanced deformation capacity, energy dissipation, and overall seismic resilience, which contributes to the ongoing development of sustainable and high-performance rehabilitation strategies for concrete structures.

Keywords: Retrofitting; Steel Plates; CFRP; ECC; Structural Sustainability; Finite Element Modeling.

1. Introduction

Reinforced concrete (RC) slabs are fundamental structural components extensively used in buildings, bridges, and various infrastructure systems. However, over time, these slabs may suffer deterioration due to aging, environmental exposure, or increasing service loads, which compromises their strength and serviceability. Consequently, retrofitting and strengthening techniques have become essential for restoring or enhancing the structural performance of such members, particularly in terms of load-carrying capacity, ductility, and durability. Previous research has focused on different strengthening strategies such as externally bonded steel plates and carbon fiber reinforced polymer (CFRP) composites [1]. More recently, engineered cementitious composites (ECC) have also attracted growing interest as an innovative material for structural rehabilitation [2]. These external bonding and overlay methods are designed to improve structural integrity and extend the service life of deteriorated concrete elements, especially RC slabs.

1.1. Overview of Retrofitting Techniques

1.1.1. Steel Plate Reinforcement

Among traditional strengthening methods, the use of externally bonded steel plates has long been recognized for its ability to enhance the flexural and shear capacities of RC members [3-5]. Steel plates offer several advantages, including

* Corresponding author: ahmedalsaadawy@engmet.edu.eg

http://dx.doi.org/10.28991/CEJ-2025-011-12-019

high tensile strength, ductility, and ease of installation, making them suitable for projects requiring rapid or large-scale retrofitting. However, limitations such as corrosion susceptibility, added self-weight, and the need for surface preparation and mechanical anchorage have restricted their long-term application [6-8]. Several studies have explored improvements in surface bonding, protective coatings, and hybrid steel–composite systems to mitigate these drawbacks [9-11]. Despite these efforts, steel retrofits remain prone to environmental degradation, motivating the exploration of more durable and lightweight alternatives [12, 13].

1.1.2. Carbon Fiber Reinforced Polymer (CFRP)

The advent of CFRP composites has revolutionized structural retrofitting due to their high strength-to-weight ratio, corrosion resistance, and ease of handling [14]. CFRP sheets, laminates, and rods are widely applied on the tension side of RC slabs using epoxy adhesives, substantially increasing flexural and shear capacities without adding significant dead load [15, 16]. Numerous studies have demonstrated that CFRP strengthening enhances load-bearing capacity, ductility, and crack control, especially in seismic regions [17-19]. Moreover, advances in adhesive and anchorage systems have minimized debonding issues, while modeling and finite element simulations have confirmed the accuracy of CFRP performance predictions [20-22]. Comparative investigations have further shown that CFRP can improve flexural strength by up to 82% relative to control specimens [18], while remaining more lightweight and durable than steel plate systems [23-25]. Despite these advantages, CFRP retrofits can face limitations related to cost, surface preparation, and long-term environmental exposure, emphasizing the need for continued material and method optimization [26-28].

1.1.3. Engineered Cementitious Composites (ECC)

In recent years, Engineered Cementitious Composites (ECC) and similar cement-based systems such as Composite Reinforced Mortars (CRM) have emerged as promising alternatives for strengthening RC structures [29, 30]. ECC exhibits strain-hardening behavior and multiple micro cracking, which significantly enhance ductility, toughness, and energy dissipation compared to conventional concrete [31-33]. Its self-healing ability through calcium carbonate precipitation in fine cracks contributes to improved long-term durability and reduced maintenance [34, 35]. Studies have shown that ECC overlays or combined ECC–FRP systems effectively enhance flexural and shear performance of RC elements [36-38]. Additionally, ECC demonstrates superior thermal resistance and better compatibility with concrete substrates than FRP, making it advantageous in repair and rehabilitation applications [39-41]. These benefits make ECC a sustainable and efficient material for strengthening slabs and other critical infrastructure.

1.2. Research Gap and Motivation

Although extensive research has been conducted on the strengthening of RC elements using steel plates, CFRP composites, and ECC materials, the existing literature still reveals several critical gaps. Most prior investigations have focused primarily on RC beams, with limited direct comparison among these three techniques when applied to RC slabs [42]. Furthermore, few studies have examined the combined structural response, ductility behavior, and long-term durability of these systems under similar boundary and loading conditions. In addition, standardized design recommendations for slab retrofitting remain insufficient, particularly regarding the selection of the most effective and sustainable technique for practical implementation.

1.3. Objectives and Novelty

To address these gaps, the present study experimentally and numerically investigates and compares the flexural performance of RC slabs retrofitted using three distinct techniques: steel plate reinforcement, CFRP sheets, and ECC with expanded mesh. The research aims to evaluate the relative effectiveness of these methods in terms of load capacity, ductility, and energy dissipation, as well as to validate finite element modeling using ABAQUS against experimental results. By conducting a direct comparison among the three strengthening methods under consistent conditions, this work contributes new insights into the optimal retrofitting strategy for RC slabs, providing a foundation for more reliable and sustainable rehabilitation design in reinforced concrete structures.

2. Research Significance and Objectives

The significance of this research lies in providing a systematic comparison of three widely adopted retrofitting techniques: steel plates, CFRP, and ECC for reinforced concrete slabs. Unlike most previous studies that focused on a single material or application method, this work combines both experimental investigations and numerical modeling to evaluate their effectiveness under similar conditions. The main objectives are: 1) To experimentally evaluate the flexural performance of RC slabs retrofitted with steel plates, CFRP, and ECC. 2) To develop and validate finite element models for predicting the behavior of retrofitted slabs. 3) To compare the advantages and limitations of each technique in terms of strength, ductility, and durability. 4) To recommend the most effective retrofitting approach for enhancing the service life of RC slabs. It should be noted that this study was limited to short-term monotonic testing. The long-term durability of ECC and CFRP systems under environmental and cyclic loading conditions warrants further investigation to validate their sustained performance in real service environments. The overall research procedure followed in this study is illustrated in Figure 1.

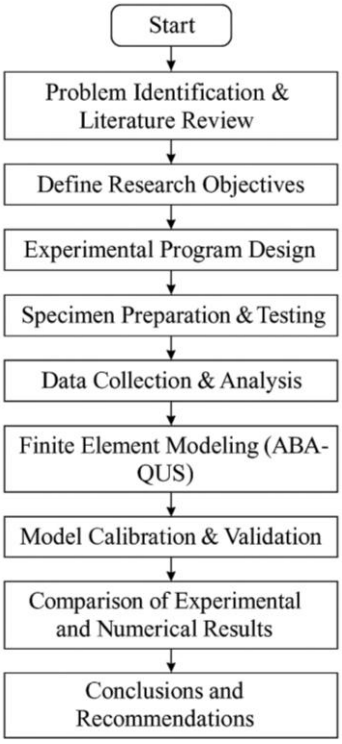

Figure 1. Research methodology flowchart

3. Program of Research

The experimental investigation focused on assessing the effectiveness of various retrofitting techniques for reinforced concrete slabs. The study involved the application of three distinct retrofitting methods: steel plates, CFRP Sheets, and ECC mortar. Initially, control specimens in the form of untreated concrete slabs were prepared and subjected to baseline testing. Subsequently, the slabs were retrofitted using each of the three techniques. Steel plates were adhesively bonded to the surface of selected slabs to enhance their load-carrying capacity. Carbon fiber plates were similarly bonded to the surface, providing high tensile strength and flexural reinforcement due to their excellent mechanical properties. Additionally, ECC mortar was applied as an overlay or embedded reinforcement layer to improve the ductility and crack resistance of the slabs. The retrofit processes involved surface preparation, application of bonding agents where necessary, and the proper placement of reinforcement materials. In the initial stage of the experimental program, ten concrete slabs with dimensions of 1000 mm × 500 mm × 50 mm were cast using a conventional concrete mixture (CO), with variations in steel reinforcement ratios. Five slabs were reinforced with 5 Ø 6 mm bars, and the remaining five with 5 Ø 8 mm bars, corresponding to steel reinforcement ratios of 0.282% and 0.502%, respectively.

After a curing period of 28 days, two slabs were tested to failure to establish the baseline behavior of un-strengthened specimens. The remaining eight slabs were randomly allocated to different retrofitting groups to minimize selection bias and ensure statistical reliability. Prior to retrofitting, these slabs were preloaded to approximately 70% of their ultimate failure load to simulate service-induced damage and flexural cracking typically observed in existing reinforced concrete elements. This preloading level was selected to induce initial cracking and moderate stiffness degradation without causing severe structural distress, thereby replicating realistic field conditions of in-service members commonly targeted for strengthening [43-46]. Subsequently, three retrofitting techniques were implemented: bonding of steel plates, application of carbon fiber-reinforced polymer (CFRP) laminates, and overlaying with an engineered cementitious composite (ECC) layer.

4. Experimental Program

4.1. Materials for Casting and Retrofitting

Two types of mixtures were employed in this study. The first was conventional concrete (CO), which was used to cast the initial slabs. The mix consisted of OPC, sand, dolomite, and water, with proportions of 350, 600, 1200, and 175 kg/m³, respectively. The second was Engineered Cementitious Composite (ECC) mortar, applied as a retrofitting layer for selected slabs (S1-E, S1-EM, S2-E, and S2-EM). The ECC mix contained sand (571 kg/m³), OPC (643 kg/m³), GGBFS (577 kg/m³), water (330 kg/m³), SP (14.8 kg/m³), and polypropylene fibers (27.3 kg/m³). The ECC mixture proportions were designed following micromechanical design principles and previous studies [47-50]. The fiber volume fraction (2%) was selected to achieve the desired strain-hardening and multiple-cracking behavior while maintaining

workability. Ground granulated blast furnace slag (GGBFS) was incorporated as a partial cement replacement (47%) to enhance environmental sustainability and optimize the strength–ductility balance. These parameters were adopted based on literature evidence demonstrating that moderate GGBFS content and controlled fiber volume fractions lead to superior tensile ductility and crack control in ECC mixes.

The particle size distribution of the fine and coarse aggregates used in the concrete mix is illustrated in Figure 2. The gradation curves were obtained through standard sieve analysis according to ASTM C136.In addition to the concrete mixtures, two external reinforcement materials were utilized. Steel sheets with a thickness of 1 mm, ultimate tensile strength of 310 MPa, and modulus of elasticity of 230 GPa were obtained from Modern Construction Chemicals Company (CMB). Carbon fiber sheets (SIKA Wrap-230C), also supplied by CMB, were employed with an ultimate tensile strength of 3000 MPa and modulus of elasticity of 200 GPa.

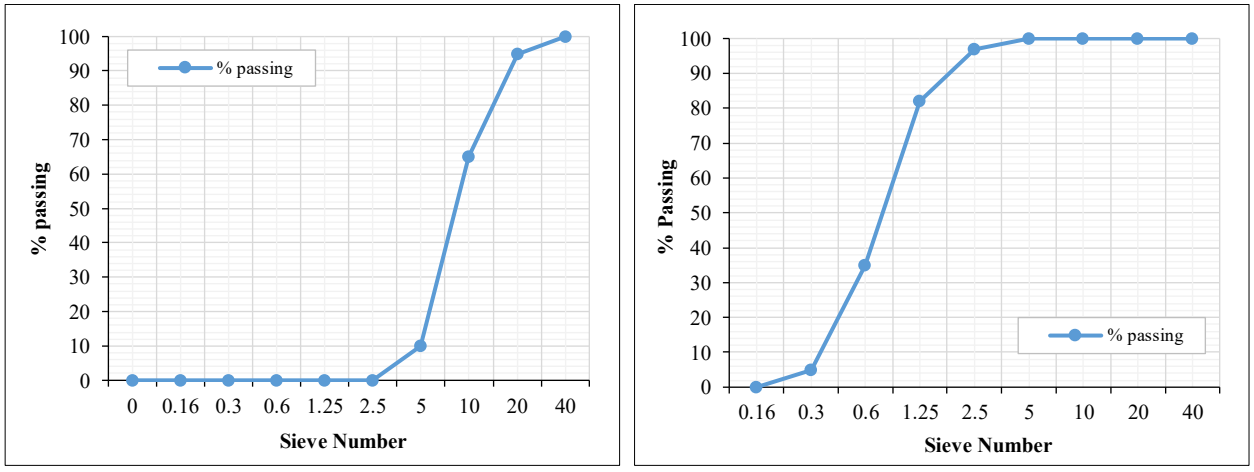

a) Coarse Aggregate **b) Fine Aggregate**

Figure 2. Particle size distribution (gradation) curves of fine and coarse aggregates

4.2. Mechanical Properties of Materials

The mechanical properties of OC and ECC were evaluated through compressive and indirect tensile (splitting) strength tests. Compressive strength was determined using 100×100×100 mm cubes according to ASTM C39 [38], while tensile strength was obtained from 100×200 mm cylindrical specimens cured for 28 days. The results indicated that ordinary concrete (OC) achieved a compressive strength of 20 MPa at 7 days and 25 MPa at 28 days, with corresponding tensile strengths of 1.2 MPa and 2.0 MPa. In contrast, engineered cementitious composite (ECC) demonstrated superior performance, reaching compressive strengths of 40 MPa at 7 days and 50 MPa at 28 days, along with tensile strengths of 4.8 MPa and 5.5 MPa, respectively. These results highlight the significantly enhanced strength and ductility of ECC compared to OC, justifying its selection as an effective retrofitting material.

4.3. Preparation of Specimens

Figure 3 illustrates the specimens utilized in the experimental investigation, consisting of ten reinforced concrete (RC) slabs. Each slab has a length of 1000 mm and a width of 500 mm, supported by two supports separated by a span of 900 mm between their centroids. According to the American Concrete Institute (ACI) 318-19 Building Code Requirements for Structural Concrete [34], the maximum reinforcement ratio (often denoted as ρ_{max}) for reinforced concrete members, including slabs, is typically limited to prevent issues such as congestion, constructability problems, and excessive reinforcement leading to brittle failure. For reinforced concrete slabs, the maximum reinforcement ratio is generally specified as equal to $0.75\rho_b$ where ρ_b is balanced reinforcement equal to 0.75% according to ACI [34]. Thus, the maximum tension reinforcement ratio was established at approximately 0.56% in accordance with the ACI 318-19 Code [34]. To induce the desired mode of flexural failure in the slabs, a reinforcement ratio was selected for ten slabs that was intentionally below this maximum value. The specimens exhibit variations in steel reinforcement ratios: five slabs are reinforced with five longitudinal bars of Φ6 mm diameter, corresponding to a reinforcement ratio of 0.282%, while the remaining five slabs are reinforced with five Φ8 mm diameter bars, corresponding to a reinforcement ratio of 0.502% with yield strengths of 280 MPa. The specimens were cast from a single concrete batch (designated as mixture CO) to eliminate variability in concrete quality. The targeted compressive strength at 28 days was specified as 25 MPa. The quantities of the constituent materials required for producing 1 m³ of concrete are summarized in Table 1. After a curing period of 28 days, two slabs were subjected to loading until failure, while the other eight slabs were loaded up to 70% of their respective ultimate failure loads. In the subsequent stage, these eight slabs, loaded to 70% of their capacity, underwent retrofitting using three different techniques: reinforcement with steel plates, reinforcement with carbon fiber plates, and application of an engineered cementitious composite (ECC) layer as illustrated in Table 1. and Figure 3.

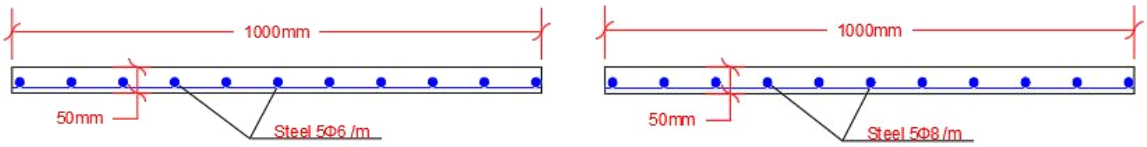

(a) (b)

Figure 3. Slabs' details (a) S1 and (b) S2

Table 1. Test specimens

Group	Slabs ID	Longitudinal Reinforcement	*ρ (%)*	*fy* (MPa)	Retrofitting Technique
	S1	5Ø6 mm	0.282	280	None
	S1-S	5Ø6 mm	0.282	280	Steel Plates
G1	S1-C	5Ø6 mm	0.282	280	CFRP
	S1-E	5Ø6 mm	0.282	280	ECC
	S1-EM	5Ø6 mm	0.282	280	ECC with welded mesh
	S2	5Ø6 mm	0.502	280	None
	S2-S	5Ø8 mm	0.502	280	Steel Plates
G2	S2-C	5Ø8 mm	0.502	280	CFRP
	S2-E	5Ø8 mm	0.502	280	ECC
	S2-EM	5Ø8 mm	0.502	280	ECC with welded mesh

4.4. Description of Repair Methods

Three strengthening techniques were adopted: steel sheets, carbon fiber-reinforced polymer (CFRP), and engineered cementitious composite (ECC), as illustrated in Figure. 4. In the steel and CFRP methods, strengthening was applied in the form of strips bonded along the longitudinal axis of the slabs with a length of 900 mm. The thicknesses and widths of the strips were chosen to provide comparable ultimate tensile capacities (~3000 MPa) based on the cross-sectional area of the strengthening materials. Steel sheet strengthening: Slabs S1-S and S2-S were retrofitted using two steel strips (50 mm × 1 mm) with a yield strength of 280 MPa bonded to the tensile face of each slab using Sikadur® epoxy adhesive (properties summarized in Table 2). CFRP strengthening: Slabs S1-C and S2-C were strengthened with SIKA Wrap-230C CFRP strips (50 mm × 0.13 mm) bonded with Sikadur® epoxy adhesive. ECC strengthening: Slabs S1-E and S2-E received a 20 mm ECC overlay applied in two layers, while slabs S1-EM and S2-EM incorporated a 10 × 10 mm steel wire mesh between the two layers. The ECC was applied over the entire tensile face after surface preparation. Table 2 summarizes the key properties of the adhesive used.

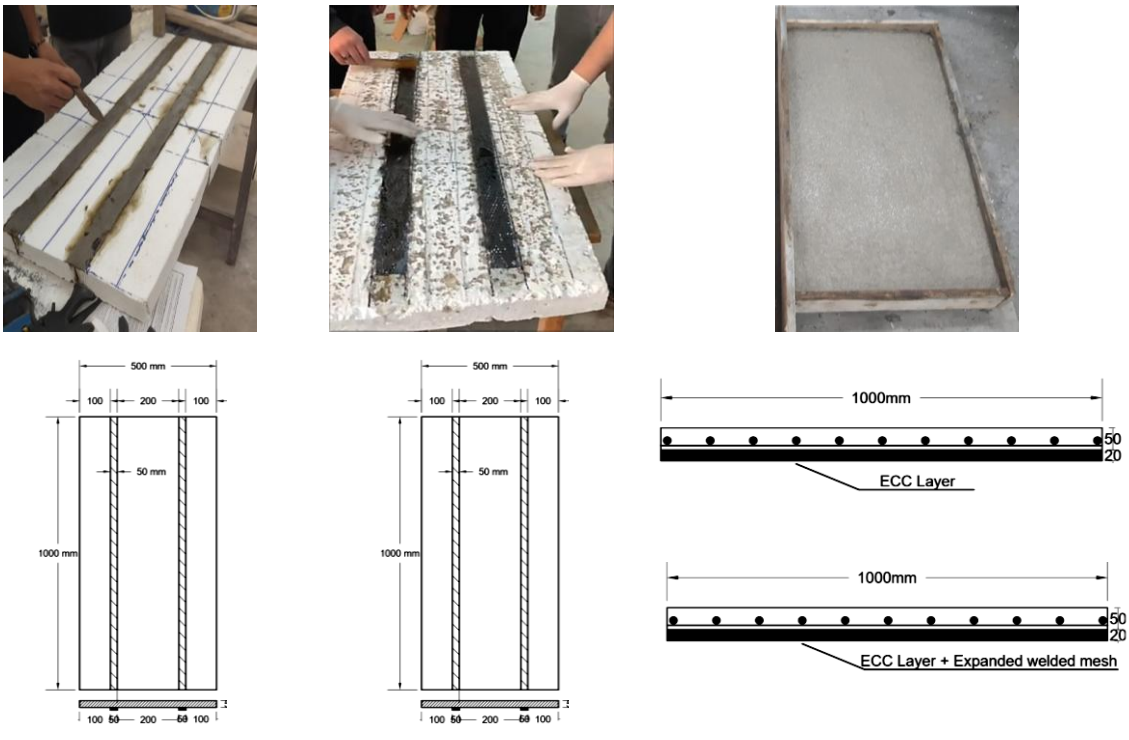

(a) **(b)** **(c)**

Figure 4. Retrofitting Techniques (a) Steel Plates, (b) CFRP and (c) ECC with and without Expanded welded mesh

Table 2. Properties of Sikadur® Adhesives

Property	Sikadur®-31 (Structural Adhesive)
Chemical Base	Two-part epoxy resin
Consistency	Thixotropic paste (non-sag)
Modulus of Elasticity in Tension	≈5,000 MPa (5 GPa)
Tensile Adhesion Strength (on concrete)	Not typically measured; used for structural bonding.
Tensile Adhesion Strength (on steel)	≈15 - 20 MPa
Compressive Strength	≈50 - 70 MPa
Main Application	Bonding concrete elements, repairing corners, filling voids, and bonding carbon fiber plates.

4.5. Test Setup

As illustrated in Figure 5, all specimens were tested using a 1000 kN universal testing machine. The slabs were simply supported over a clear span of 900 mm (Figure 5-a). The applied load was transferred through two steel plates spaced 300 mm apart and centered along the slab axis, ensuring symmetric loading conditions. The distance between the edges of the load plates and the nearest supports was maintained at 300 mm. Deflections were continuously monitored using linear variable differential transformers (LVDTs). One LVDT was placed at the mid-span and another at one-third span (Figure 5-b). Measurements were recorded at every load increment of 0.5 kN. For each specimen, the load corresponding to the first visible crack was also documented.

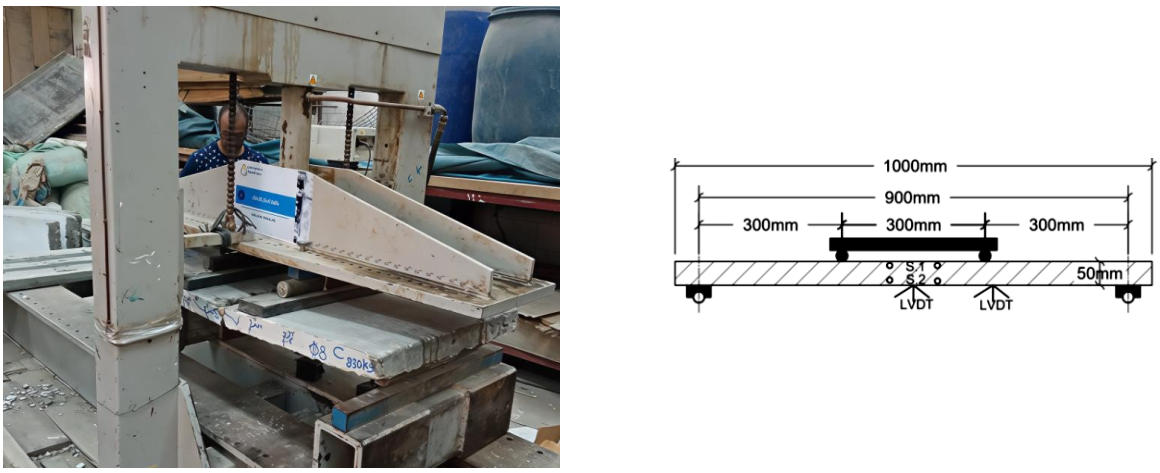

(a) **(b)**

Figure 5. Experimental configuration of the specimen

Un-strengthened control specimens were tested to ultimate failure. In contrast, retrofitted slabs were first loaded up to approximately 70% of their ultimate capacity, consistent with previous studies [43–46]. After unloading, the strengthening techniques described earlier were applied, and the slabs were reloaded until failure. It is worth noting that the appearance of the first crack marks the transition from linear-elastic to nonlinear structural behavior. Applying retrofitting at service-level loads (70% of ultimate) is considered more representative of realistic structural performance.

5. Results and Analytical Discussion of Slab Performance

5.1. Failure Modes and Crack Characteristics

Crack initiation and development were systematically observed following each increment of applied load. In the case of the un-strengthened reference slabs, designated as S1 and S2, the first visible cracks appeared at applied forces of 2.2 kN and 4.7 kN, respectively, corresponding to approximately 44% and 46% of their respective collapse loads. As the load increased, a pattern of flexural cracking emerged at the midpoint of the slabs, with cracks propagating longitudinally and transversely toward the edges. Over time, these primary cracks widened and were accompanied by the formation of additional cracks. This progressive cracking led to a reduction in the stiffness of the slabs, evident through substantial central deflections occurring with only marginal increases in load near the ultimate capacity, around 5.0 kN for S1 and 10.2 kN for S2. The failure mode for both S1 and S2 was characterized as flexural failure, as illustrated in Figure 6.

(a) (b)

Figure 6. Mode failure and crack pattern (a) S1 and (b) S2

In the case of the slabs, designated as S1-S and S2-S, the first visible cracks appeared at applied forces of 2.4 kN and 4.0 kN, respectively, corresponding to approximately 57% and 44.44% of their respective collapse loads. During the loading process, elevated shear and tensile stresses developed along the interface between the steel plate and the concrete surface, particularly in regions of stress concentration such as load application points and the plate edges. When these interfacial stresses surpassed the bond strength of the adhesive, debonding initiated, as illustrated in Figure 7. The onset of debonding resulted in the loss of effective stress transfer by the steel plate, leading to a significant decrease in the retrofit's load-carrying capacity and potentially causing abrupt structural failure. The ultimate capacity reached 4.2 kN for S1-S and 9.0 kN for S2-S. The collapse of the slabs retrofitted with CFRP occurred as a result of fracture and separation within the CFRP layer. These fractures propagated, weakening the bond between the CFRP and the concrete substrate, leading to the eventual separation of the CFRP layer. As the CFRP layer was tensioned and peeled away from the slab, its capacity to reinforce and distribute loads was compromised, causing the structural integrity to deteriorate rapidly. For the retrofitted slabs designated as S1-C and S2-C, the initial visible cracks were observed at applied forces of 3.1 kN and 8.2 kN, respectively. These load levels correspond to approximately 50.8% and 50.6% of their respective ultimate collapse loads, which are approximately 6.1 kN for S1-C and 16.2 kN for S2-C, as shown in Figure 8.

(a) (b)

Figure 7. Mode failure and crack pattern (a) S1-S and (b) S2-S

(a) (b)

Figure 8. Mode failure and crack pattern (a) S1-C and (b) S2-C

The failure mechanism of retrofitted slabs reinforced with ECC mortar predominantly manifested as the development of a prominent crack located in the mid-span region along the transfer (longitudinal) direction, as shown in Figure 9. This crack indicated a localized loss of structural integrity, typically resulting from tensile stress concentrations that exceeded the ductile capacity of the ECC layer. The formation of such a crack disrupted the load transfer mechanism between the retrofitted layer and the substrate, thereby increasing the risk of brittle failure or collapse of the slab. In the case of the retrofitted slabs designated as S1-E and S2-E, initial visible crack initiation was observed at applied forces of 3.0 kN and 5.0 kN, respectively. These load levels represented approximately 50% and 45.045% of their respective ultimate load capacities, which were approximately 6.0 kN for S1-E and 11.1 kN for S2-E.

(a) (b)

Figure 9. Mode failure and crack pattern (a) S1-E and (b) S2-E

The flexural failure mechanism of the slabs retrofitted with ECC mortar and expanded welded mesh was predominantly governed by strain localization and crack propagation under bending stresses. As the applied load increased, tensile stresses concentrated at the tension face of the slab, initiating micro-cracks within the ECC layer owing to its high strain capacity and crack control properties. In the cases of slabs S1-EM and S2-EM, micro-cracks were first observed at applied forces of 3.0 kN and 6.6 kN, respectively, corresponding to approximately 49.1% and 48.5% of their respective ultimate loads. These micro-cracks gradually coalesced into a dominant crack propagating across the mid-span region, leading to significant weakening of the tension zone. The incorporation of expanded welded mesh provided additional reinforcement, aiding stress distribution and improving ductility. However, under excessive loading, the combined effects of crack growth in the ECC mortar and the yielding or rupture of the welded mesh precipitated a sudden decline in structural capacity. This failure mechanism, as depicted in Figure 10, was characterized by large deflections and the formation of a prominent crack across the span, ultimately resulting in flexural failure.

(a) (b)

Figure 10. Mode failure and crack pattern (a) S1-EM and (b) S2-EM

5.2. Structural Response under Load and Deflection

Figure 11. illustrates the effect of the implemented strengthening techniques on the load-deflection behavior of the slabs. A detailed examination of the figure indicates that the application of steel plates, as observed in slabs S1-S and S2-S, respectively, did not produce a significant alteration in the load-deflection response when compared to the un-strengthened control slabs S1 and S2. This occurred due to sudden failure of the interface between the steel reinforcement layer and the concrete slab, primarily due to insufficient bonding of the existing bonding material. To ensure an effective bond between the reinforcement and the concrete substrate, it is recommended to utilize an adhesive bonding agent in conjunction with mechanical fastening methods such as nails. However, in this case, the use of nails was not implemented because the slab had prior loading history, exhibited initial cracking, and had a limited thickness. These factors raised concerns regarding the potential for slab fracturing during nail installation, which could adversely affect the integrity of the laboratory testing results.

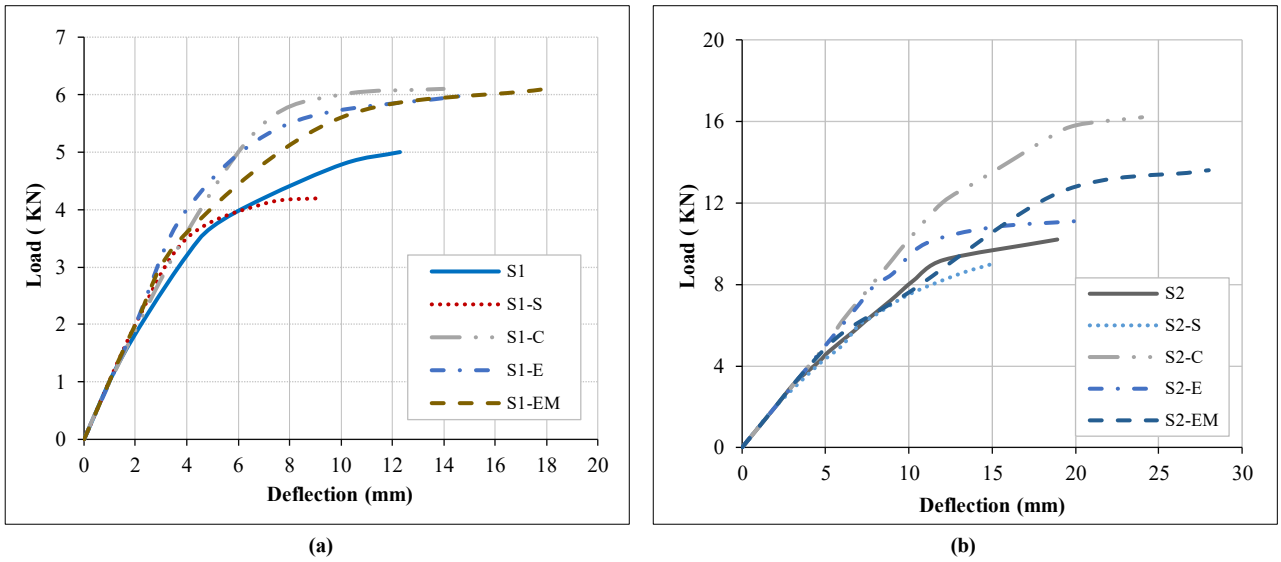

(a) (b)

Figure 11. Load–deflection behavior of the slabs: (a) Group 1 and (b) Group 2

Conversely, S1-C and S2-C, which were retrofitted by CFRP, exhibited distinctly different load–deflection responses compared to the other specimens due to their flexural failure mode, as illustrated in Figure 11. The load–deflection behavior of these two slabs can be characterized by three discernible phases: (1) the elastic (stiffest) stage, during which a proportional relationship was observed between the central deflection and the increment in applied load, extending approximately up to 37% and 42% of their respective failure loads; (2) the plateau phase, characterized by significant deflections with only marginal increases in applied load, which continued until reaching the peak load; and (3) the descending phase, marked by abrupt reductions in load-carrying capacity shortly after reaching the ultimate load. Notably, slabs S1-C and S2-C achieved the highest peak loads among all ten specimens, indicating superior flexural capacity. Similar multi-stage responses have been reported by Breveglieri & Czaderski [48], who observed that externally bonded CFRP laminates substantially increase both ultimate strength and post-cracking stiffness of RC slabs, confirming that the CFRP retrofit effectively enhances load redistribution and energy absorption capacity.

In contrast, slabs retrofitted with ECC mortar, either with or without expanded welded mesh, exhibited enhanced ductility and a smoother post-peak response, signifying improved deformability and progressive failure. The superior performance of ECC-based retrofits can be attributed to their inherent strain-hardening and multiple micro cracking behavior, which enable the material to sustain significant tensile strain while maintaining load-carrying capacity. These findings align with the studies of Yang et al. [49], who demonstrated that ECC overlays delay crack localization and significantly improve the ductility and toughness of RC members under flexural loading. When expanded welded mesh was embedded within the ECC layer, an even greater improvement in load-carrying capacity and ductility was recorded. The mesh serves as an additional reinforcement medium, enhancing tensile stress distribution and bridging wider cracks. This synergistic effect is consistent with the experimental results reported by Ahamed et al. [50] who found that combining ECC with steel or polymeric meshes can enhance both flexural resilience and energy dissipation by more than 50% compared to plain ECC overlays.

Quantitatively, the maximum deflections at failure for strengthened slabs increased by 13.8–46.3% relative to control slab S1 and by 5.8–48% relative to control slab S2, highlighting the significant gains in deformability and energy absorption. However, steel plate–retrofitted slabs exhibited limited improvements, primarily due to premature interfacial debonding that restricted composite action. Overall, the experimental findings reinforce that CFRP provides the highest strength enhancement, while ECC–mesh systems deliver the most balanced improvement in ductility and energy absorption, demonstrating a robust retrofitting alternative for sustainable and resilient RC structures.

5.3. Cracking and Load Capacity

Figure 12 illustrates the cracking load and ultimate load capacities for the ten evaluated slabs, while Figure 13. emphasizes the effectiveness of the proposed strengthening techniques in restoring the capacity lost due to initial damage. Together, these figures highlight the improvements in strength achieved using different retrofitting materials.

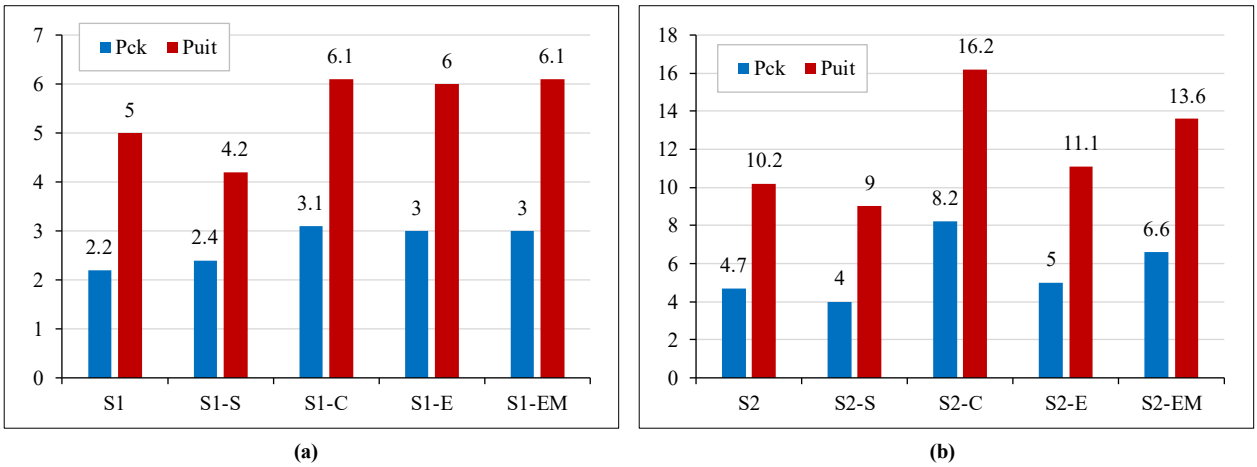

Figure 12. Ultimate and Cracking load (a) Group1 and (b) Group2

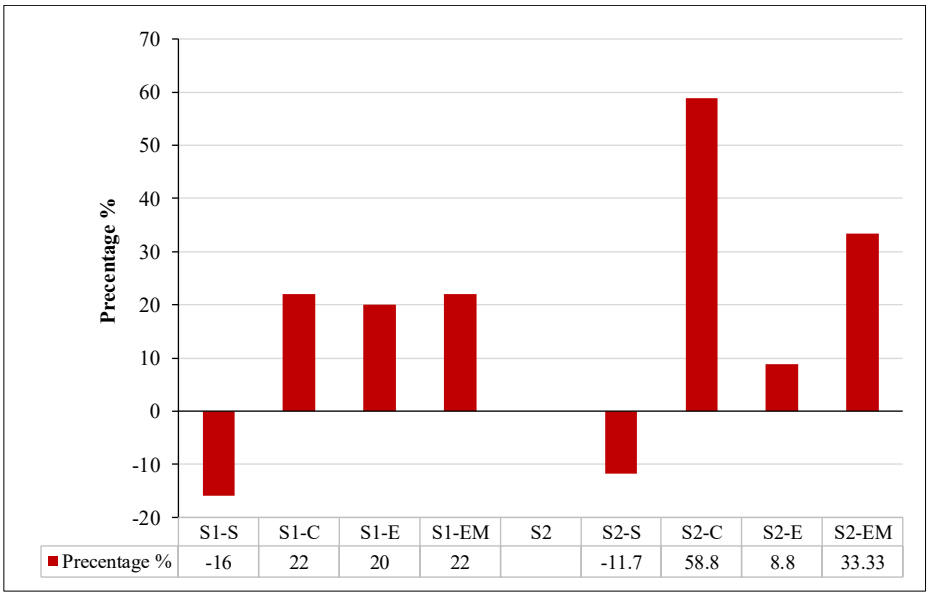

Figure 13. Percentage increase in the ultimate load capacities of the retrofitted slabs compared to the un-retrofitted specimens S1 and S2

The most effective strengthening method was the application of CFRP sheets, which resulted in strength enhancements of 22.0% and 58.8% relative to the control specimens with holes, S1 and S2, respectively. Moreover, incorporating a layer of ECC mortar combined with expanded welded mesh also yielded notable improvements in the ultimate load capacity, increasing it by 22% and 33% compared to the control slabs S1 and S2, respectively.

Conversely, retrofitting the slabs with steel plates resulted in a reduction of the ultimate load capacity by 16% and 11.7% compared to the control slabs S1 and S2. This premature failure was attributed to inadequate bonding between the steel plates and the concrete slab. Therefore, enhancing the connection by incorporating mechanical fastening elements such as nails is recommended to improve bond quality and structural performance. In summary, CFRP sheets and ECC mortar with welded mesh proved to be the most effective retrofitting methods for restoring slab capacity, achieving substantial improvements. Conversely, steel plate retrofitting was less effective due to bonding issues, highlighting the importance of proper connection techniques for successful structural reinforcement.

The most effective strengthening method was the application of CFRP sheets, which produced substantial enhancements in ultimate load capacity 22.0% and 58.8% relative to the control slabs S1 and S2, respectively. This significant improvement can be attributed to the superior tensile strength, high stiffness-to-weight ratio, and strong adhesive bond of CFRP with the concrete substrate, which collectively improve flexural resistance and delay crack propagation. These findings are consistent with the results of Breveglieri & Czaderski [48], who reported strength gains in the range of 20–60% for CFRP-strengthened RC slabs under flexural loading. Similarly, Samarakoon et al. [46] observed that CFRP reinforcement effectively restrains crack growth and enhances post-yield behavior, confirming the efficiency of this strengthening technique for flexural applications.

In comparison, the use of engineered cementitious composite (ECC) mortar combined with expanded welded mesh also produced notable gains in ultimate load—22% and 33% relative to control slabs S1 and S2, respectively. The improvement stems from the strain-hardening and multiple micro cracking behavior of ECC, which provides enhanced tensile ductility and superior crack control. The embedded welded mesh further contributes to the load transfer and confinement mechanism, promoting distributed cracking and delaying failure. These synergistic effects are in agreement with findings by Yang et al. [49] who demonstrated that hybrid ECC–mesh retrofitting systems can increase flexural capacity by up to 35% while substantially improving ductility and energy absorption.

Overall, the experimental observations confirm that CFRP remains the most effective retrofitting method in terms of strength enhancement, while ECC–mesh systems offer a well-balanced improvement across strength, ductility, and crack control—making them a promising alternative for sustainable and resilient strengthening applications.

5.4. Ductility

Ductility, a key parameter reflecting the structural performance under flexural loads, was quantified using the ductility index, defined as the ratio of the maximum mid-span deflection at failure to the deflection at steel yield [9]. Tables 3 and 4 present the ductility values for the control and retrofitted slabs. The results indicate that retrofitting with CFRP sheets and ECC mortar combined with expanded mesh positively influenced the ductility of the slabs. Specifically, specimens S1-C and S2-C exhibited approximately 10.2% and 3.2% higher ductility compared to S1 and S2, while S1-EM and S2-EM demonstrated substantial increases of 43% and 6.1%, respectively.

Conversely, the application of steel plates for retrofitting led to a decrease in ductility of 2.4% and 8.7% relative to the control slabs S1 and S2, respectively. These findings highlights that retrofitting methods such as CFRP sheets and ECC mortar with expanded mesh significantly improve the ductility of reinforced concrete slabs, enhancing their flexibility and energy absorption capacity under flexural loading. Conversely, steel plate retrofitting marginally reduces ductility, indicating that different strengthening techniques can have varying impacts on structural performance.

5.5. Energy Absorption

The energy absorption capacity, denoted as J and calculated as the area under the load–deflection curve, serves as a critical indicator of the structural resilience of the tested slabs. As shown in Tables 3 and 4, the retrofitting interventions with CFRP sheets and ECC mortar combined with expanded mesh significantly enhanced the energy absorption capacity of the slabs. Specifically, specimens S1-C and S2-C exhibited approximately 45.2% and 95.23% increases in J compared to control specimens S1 and S2, respectively, while specimens S1-EM and S2-EM demonstrated substantial increases of 90.7% and 97.6%, respectively. Conversely, the application of steel plates for retrofitting led to a decrease in energy absorption capacity by 35.9% and 34.5 % relative to the control specimens S1 and S2, respectively.

Table 3. Summary of the experimental results for the tested slabs

Group	Specimen	Cracking Stage		Ultimate Stage			K (kN/mm)	K/K (control)	J (kN.mm)	Δ_u/Δ_{cr}
		P_{cr} (kN)	Δ_{cr} (mm)	P_u (kN)	P_u/P_u (Control)	Δ_{pu} (mm)				
G1	S1	2.2	3	5	1	12.3	0.73	1	43.048	4.1
	S1-S	2.4	2.3	4.2	0.84	9.2	1.043	1.43	28.03	4.0
	S1-C	3.1	3.1	6.1	1.22	14	1.0	1.37	62.5	4.52
	S1-E	3	3.1	6	1.2	15	0.97	1.33	67.25	4.84
	S1-EM	3	3.07	6.1	1.22	18	0.98	1.34	82	5.86
G2	S2	4.7	6.1	10.2	1	18.91	0.77	1	127.482	3.10
	S2-S	4	5.3	9	0.88	15	0.75	0.97	83.5	2.83
	S2-C	8.2	7.5	16.2	1.59	24	1.093	1.42	248.88	3.2
	S2-E	5	5.2	11.1	1.1	20	0.96	1.24	155.1	3.85
	S2-EM	6.6	8.5	13.6	1.33	28	0.78	1.01	251.92	3.29

P_{cr}: First crack load, Δ_{cr}: Deflection at the onset of first cracking P_u: Ultimate load, Δ_{pu}: Deflection at failure, K: Elastic stiffness index (kN/mm), J: Energy absorption capacity (kN·mm).

Table 4. Comparative summary of performance improvements for retrofitted slabs relative to control specimens

Retrofitting Technique	Change in Ultimate Strength (%)	Change in Ductility (%)	Change in Energy Absorption (%)	Overall Performance Remarks
(S1, S2)	—	—	—	Baseline specimens; early crack initiation (~44–46% of ultimate load).
(S1-S, S2-S)	↓ 11–16%	↓ 2–9%	↓ 34–36%	Poor bond performance led to interfacial debonding and premature failure; reduced ductility and energy dissipation.
(S1-C, S2-C)	↑ 22–58.8%	↑ up to 40%	↑ up to 97%	Highest strength gain and energy absorption; distinct three-phase load–deflection response; failure by CFRP fracture or separation.
(S1-E, S2-E)	↑ Moderate (approx. 15–25%)	↑ Moderate (~20–30%)	↑ 40–60%	Improved stress redistribution and controlled crack propagation; gradual post-peak response.
(S1-EM, S2-EM)	↑ 22–33%	↑ up to 43%	↑ up to 97%	Provided enhanced confinement and resilience; promoted micro-cracking before coalescence; best overall ductility-energy balance.

In summary, retrofitting with CFRP sheets and ECC mortar combined with expanded mesh markedly improves the energy absorption capacity of reinforced concrete slabs, significantly enhancing their structural resilience. In contrast, steel plate retrofitting results in a substantial reduction in energy absorption, indicating that different strengthening methods have varying impacts on the slabs' ability to dissipate energy under load.

5.6. Comparative Summary of Results

Table 4 shows the comparative summary of percentage improvements in ultimate strength, ductility, and energy absorption for different retrofitting techniques relative to the control slabs. CFRP and ECC mesh retrofitting demonstrated the most significant gains in both ductility and energy dissipation, while steel plate retrofitting showed reduced performance due to interfacial debonding.

Based on a combined assessment of ultimate strength, ductility, and energy absorption, the CFRP system demonstrated the highest overall performance, followed closely by the ECC–mesh retrofit, which offered superior crack control and post-peak ductility as shown in Table 5. The steel plate system ranked lowest due to premature interface failure and reduced overall efficiency.

Table 5. The overall ranking of performance improvements for retrofitted slabs

Rank	Retrofitting Method	Overall Performance Summary
1	CFRP Plates	Highest strength gain and energy dissipation; good ductility; efficient bond behavior until failure.
2	ECC + Mesh Overlay	Excellent ductility and energy absorption; moderate-to-high strength gain; superior crack control and post-peak resilience.
3	Steel Plate Bonding	Decreased strength, ductility, and energy capacity due to premature debonding and weak interface behavior.

6. Numerical Study

The theoretical framework of the present research is based on nonlinear finite element analysis (FEA) principles, which provide a powerful tool for understanding the flexural response and damage evolution of reinforced concrete (RC) slabs under strengthening and loading conditions. The adopted modeling approach relies on the continuum mechanics theory, where concrete and composite materials are treated as heterogeneous but isotropic media governed by plasticity and damage evolution laws.

The Concrete Damage Plasticity (CDP) model is selected as the theoretical foundation to describe the inelastic behavior of concrete in both tension and compression, capturing stiffness degradation and post-cracking responses. The model accounts for the combined effects of tensile cracking and compressive crushing, allowing the simulation of stiffness recovery and energy dissipation during cyclic loading. The numerical modeling of retrofitted slabs integrates experimental parameters such as material strengths, geometry, and boundary conditions, ensuring that the theoretical predictions accurately reflect the real structural behavior observed in laboratory tests.

This theoretical approach establishes a consistent framework linking the experimental investigation and the numerical simulation, enabling validation of the proposed retrofitting techniques and assessment of their influence on load-carrying capacity, deformation characteristics, and overall structural ductility.

A numerical study was conducted using Abaqus [39] software to complement the experimental investigation of retrofitting RC slabs with different reinforcing strategies, including steel plates, CFRP plates, and ECC layers. Ten finite element models were developed to capture the nonlinear behavior of concrete and steel reinforcement. The study explored bond–slip behavior, load transfer, and potential failure modes such as debonding, steel plate yielding, CFRP plate debonding, and ECC–concrete interaction.

Material models accounted for concrete crushing, reinforcement yielding, and strain-hardening or damage behavior in the retrofit materials. The slab model simulated in Abaqus comprised ordinary concrete, ECC, steel reinforcement bars, steel plates, and CFRP sheets under support and loading conditions. The concrete slab and ECC layers were modeled using C3D8R elements, representing homogeneous solid brick elements with 8 nodes. Each node possesses three translational degrees of freedom, and the element utilizes reduced integration to compute the stiffness matrix incrementally during load application. Reinforcement bars and welded steel mesh were represented using T3D2 truss elements, featuring two nodes with three degrees of freedom per node. Steel plates and CFRP sheets were modeled as a composite layup using S4R shell elements, a 4-node doubly curved thin shell with reduced integration. Embedded regions were assigned to steel rebar's within the concrete host material. The CFRP sheets were connected to the concrete slab via a tie constraint, with the concrete slab defined as the master surface and the CFRP sheet as the slave surface.

A uniform mesh with a characteristic element size of 10 mm was employed across all components to achieve an optimal compromise between computational efficiency and solution accuracy, as illustrated in Figure 14.

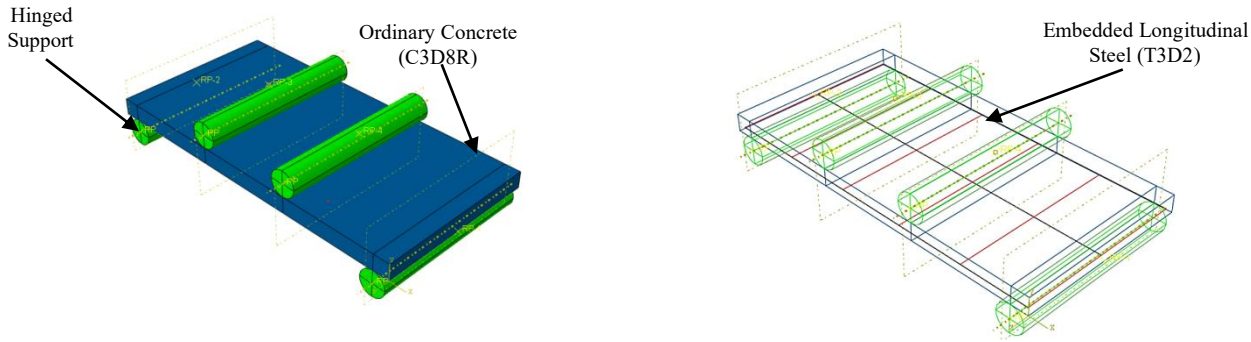

(a) Geometry of slabs and steel

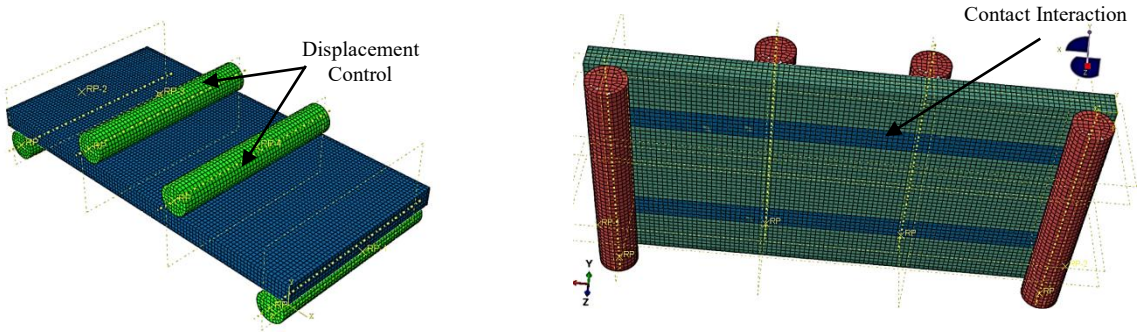

(b) Finite Element mesh

Figure 14. Numerical model details

6.1. Material Properties

The compressive strength adopted for modeling the ordinary concrete in the slab is 25MPa, and the cracking stress is taken as 40% of the compressive strength, consistent with experimental observations. Consequently, concrete is represented in Abaqus with two mechanical behaviors: a linear elastic response characterized by the elastic modulus and Poisson's ratio, and a plastic response described in two stages—strain hardening up to the concrete strength followed by strain softening beyond the peak strength. The Concrete Damage Plasticity (CDP) model is employed to define the post-cr cracking behavior of concrete [40, 41]. The compressive stress–strain relationship of the concrete is formulated using the Hognestad curve, as given in Equation 1, which provides a reasonable fit to the experimental results.

$$\sigma_c = 2f_c' \left[\frac{\varepsilon_c}{\varepsilon_{co}} - \left(\frac{\varepsilon_c}{\varepsilon_{co}}\right)^2\right] \quad (1)$$

where, σ_c is the concrete compressive stress at the corresponding strain (ε_c) in MPa, ε_c is the concrete strain at compression, and (ε_{co}) is the strain at the compressive strength.

Poisson's ratios is 0.20 for ordinary concrete (OC) and 0.18 for engineered cementitious composite (ECC). The Concrete Damage Plasticity (CDP) model available in ABAQUS was employed to capture nonlinear concrete behavior. The CDP parameters are summarized in Table 6. For reinforcing steel was Modeled as an elastic–perfectly plastic material with an elastic modulus of 200GPa. Longitudinal reinforcement bars were assigned to a yield stress of 280 MPa. Ultimate Tensile Strength=310 MPa, and Modulus of Elasticity = 230 GPa of Steel plates.

Table 6. The CDP model's parameters for OC and ECC

Types	Dilation angle (ψ)	Eccentricity (e)	Shape parameter (K_c)	Maximum compression axial/biaxial (f_{bo}/f_{co})	Viscosity (μ)
OC	37	0.1	2/3	1.16	0
ECC	39	0.1	2/3	1.16	0

Elastic and plastic states are used to model CFRP sheets. Hashin Damage is used to determine the plastic behavior and Lamina type for the elastic behavior. fiber-reinforced composites' damage characteristics. The manufacturer's experimental values are what determine the calibrated data. Table 7 lists the CFRP sheets' mechanical characteristics. where μ12 is the Poison's ratio in the xy plane, G12, G13, and G23 are the shear modulus in the xy, xz, and yz directions, while E1 and E2 are the elastic modulus in the x and y directions [42].

Table 7. The CFRP sheets' mechanical characteristics when utilized in Abaqus

Elastic	E1(MPa)	E2(MPa)	μ12	G12, (MPa)	G13 (MP)	G23 (MPa)
	131950	9610	0.336	5280	7020	3290
Hashin Damage						
Long. Tensile strength		**Long. Compressive strength**	**Transverse tensile strength**	**Transverse compressive strength**	**Long. Shear strength**	**Transverse shear strength**
1338 MPa		1074 MPa	71.9 MPa	231 MPa	70.2 MPa	92.5 MPa
Plastic	**Damage Evolution type Energy softening linear**					
Longitudinal tensile fracture energy		**Longitudinal compressive fracture energy**	**Transverse tensile fracture energy**		**Transverse compressive fracture energy**	
340 J/m^2		340J/m^2	2100J/m^2		2100J/m^2	

Two distinct methods could be used to assess the interaction between CFRP and concrete. The overall workflow adopted for the finite element modeling and simulation process is summarized in Figure 15. The first took into account the possibilities of merging tie constraints. According to a study by Jin et al. [43], two dissimilar surfaces (master concrete surface, slave CFRP surface) should not move relative to one another. The cohesive zone model for this search was used in a simulation as the second technique. Because it prevents the transfer of tensile stresses across the interface by reducing the expansion of the slave surface into the master surface at the constraint points, the "hard" contact relationship was selected for this simulation. Table 8 is a list of the epoxy resin parameters used in this numerical research.

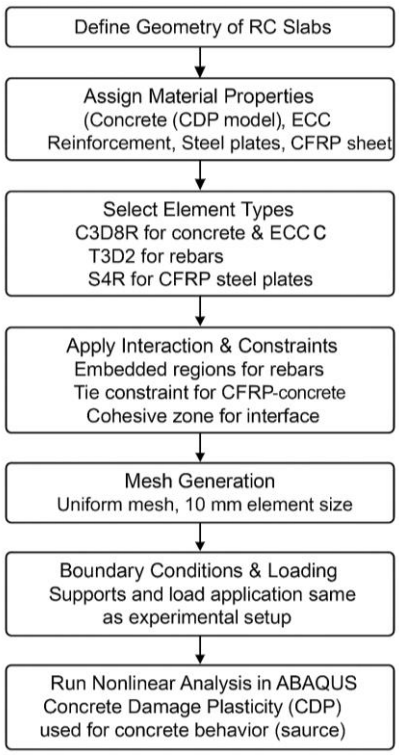

Figure 15. Flowchart of the finite element modeling workflow

Table 8. Mechanical characteristics of the interaction between CFRP and concrete

Normal stiffness, K_{nn} (MPa/m)	Shear stiffness, K_{ss} (MPa/m)	Shear stiffness, K_{tt} (MPa/m)	Normal strength, $\sigma_n(MPa)$	Shear-1 strength, $\tau_t(MPa)$	Shear-2 strength, $\tau_s(MPa)$
1830×10^3	500×10^3	500×10^3	4.05	8.782	8.782
Normal fracture energy, $G_{nn}(J/m^2)$	**1st Shear fracture energy, $G_{ss}(J/m^2)$**	**2nd Shear fracture energy, $G_{tt}(J/m^2)$**	**Benzeggagh-Kenane exponent, η**	**Stabilization**	
90	900	900	1.45	0.00001	

6.2. Results of Numerical Analysis

This FEM technique effectively captured the nonlinear flexural response and progressive cracking of the retrofitted slabs. Figures 16 and 17 display the results of the slab finite element simulation, while Table 9 provides a comparative analysis. Key parameters, including Pu (ultimate load), and Δu (ultimate deflection), are summarized in Table 9, along with their mean values and standard deviations. These parameters were used to quantitatively evaluate the correlation between experimental data and FEM predictions. The simulated load-deflection responses represented all major behavioral stages observed in the experimental testing: the initial elastic stage (representing stiffness), crack initiation, yield progression, and ultimate failure. A close match was observed across all phases, indicating that the numerical model accurately represents the structural behavior of the retrofitted slabs under flexural loads.

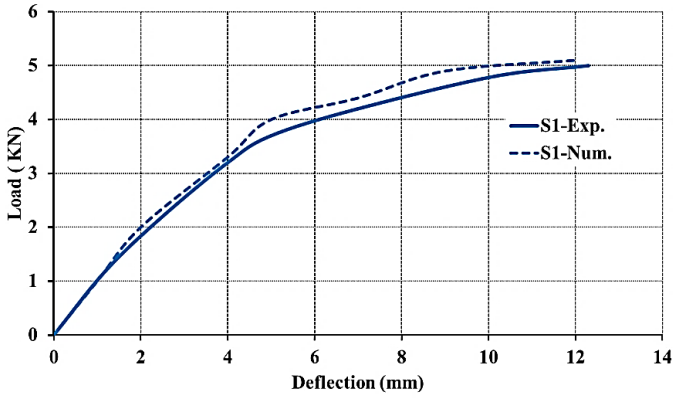

(a)

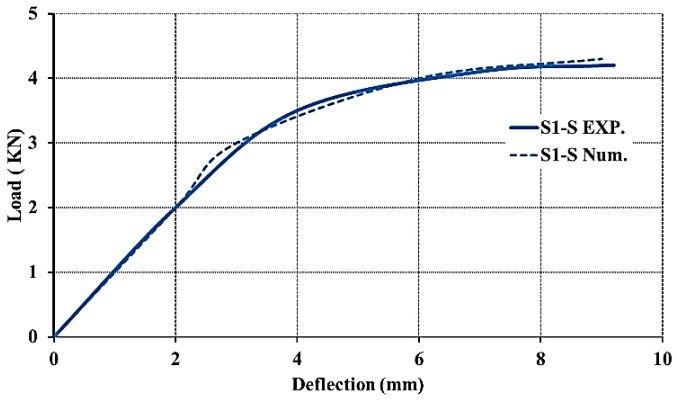

(b)

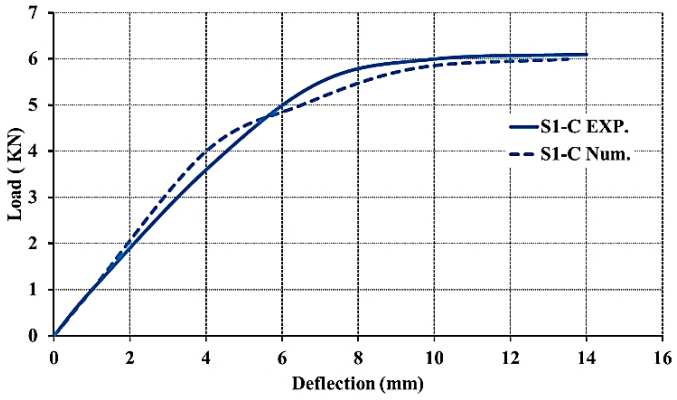

(c)

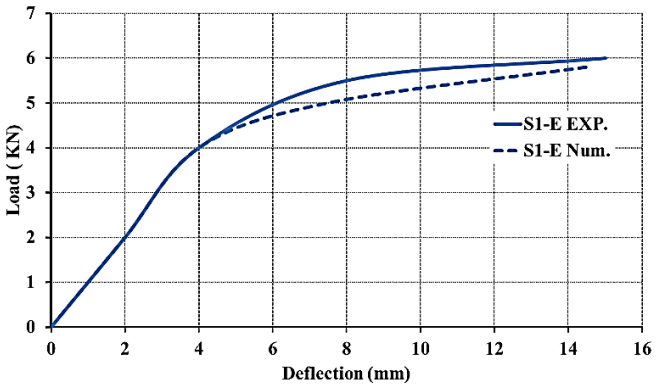

(d)

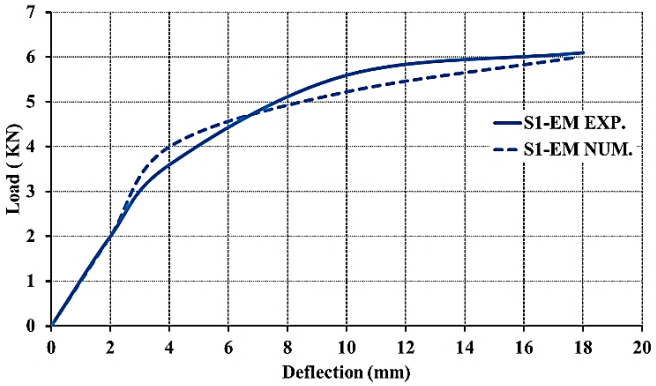

(e)

Figure 16. Load-deflection behavior for slabs in group 1 compared to experiments

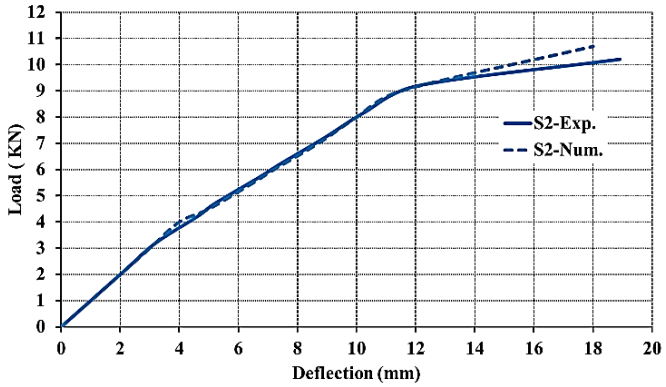

(a)

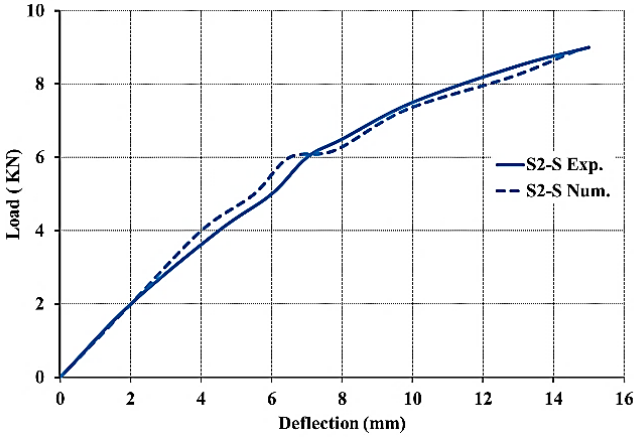

(b)

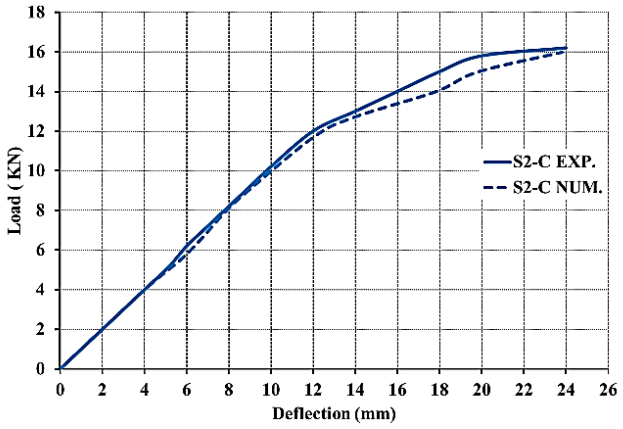

(c)

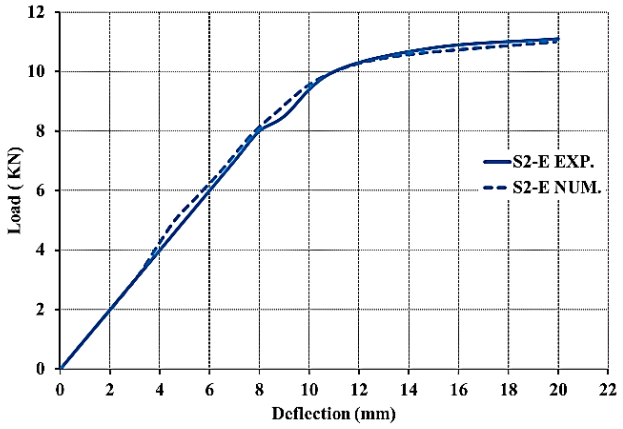

(d)

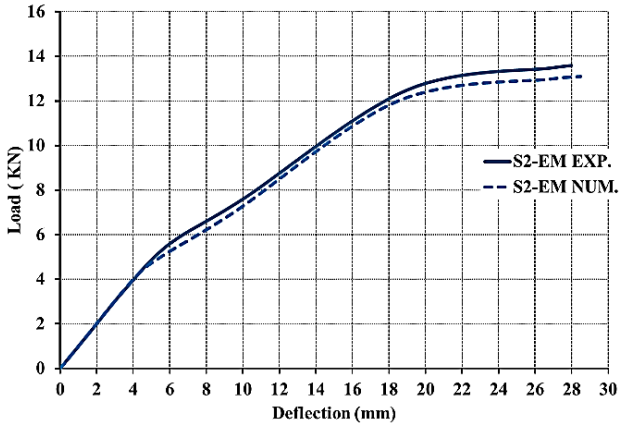

(e)

Figure 17. Load-deflection behavior for slabs in group 2 compared to experiments

Table 9. Comparison of the experimental and numerical results

Group	Specimen	P_u (KN)			Δ_{Pu}(mm)		
		Exp.	Num.	Exp./ Num.	Exp.	Num.	Exp./ Num.
G1	S1	5	5.1	0.98	12.3	12	1.03
	S1-S	4.2	4.3	0.98	9.2	9	1.02
	S1-C	6.1	6	1.02	14	13.5	1.04
	S1-E	6	5.8	1.03	15	14.5	1.03
	S1-EM	6.1	6	1.02	18	17.8	1.01
G2	S2	10.2	10.7	0.95	18.91	18	1.05
	S2-S	9	8.9	1.01	15	14.6	1.03
	S2-C	16.2	16	1.01	24	23.8	1.01
	S2-E	11.1	11	1.01	20	19.9	1.01
	S2-EM	13.6	13.1	1.04	28	28.5	0.98
Avg				1.04			1.021
SD				0.027			0.0196

The experimental data and numerical results show strong agreement. The average ratio between the FEM-predicted and empirically measured ultimate load is 1.005, with a standard deviation of 0.027 (Table 9), indicating that the proposed FEM model can accurately and reliably predict the flexural capacity of reinforced concrete retrofitting slabs. Moreover, the simulations accurately replicated the failure mechanisms observed in the tests. Crack propagation patterns and the dominant failure modes—flexural failure and debonding of CFRP and steel plates were successfully captured in the simulations (Figures 18 and 19). These findings validate the modeling approach for capturing both the progression of localized damage and the overall behavior of reinforced concrete slabs.

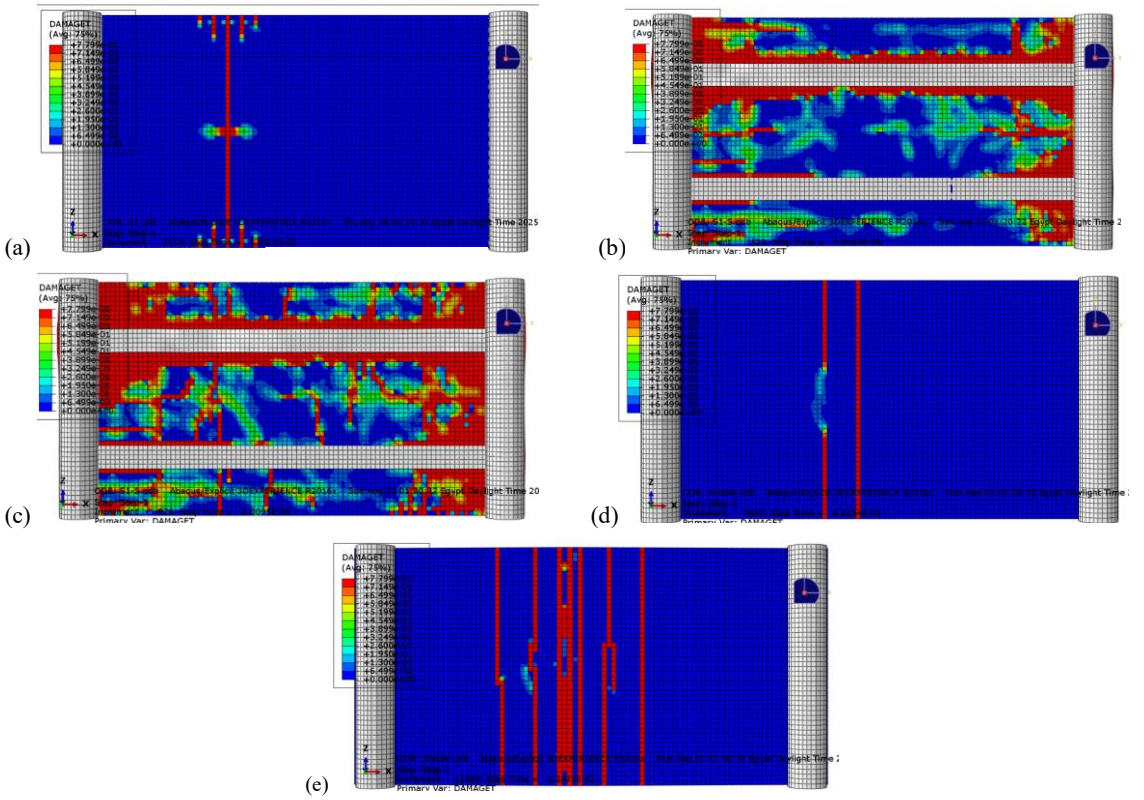

Figure 18. FEM failure mode of Slabs in group 1; (a) S1, (b) S1-S, (c) S1-C, (d) S1-E, and (d) S1-EM

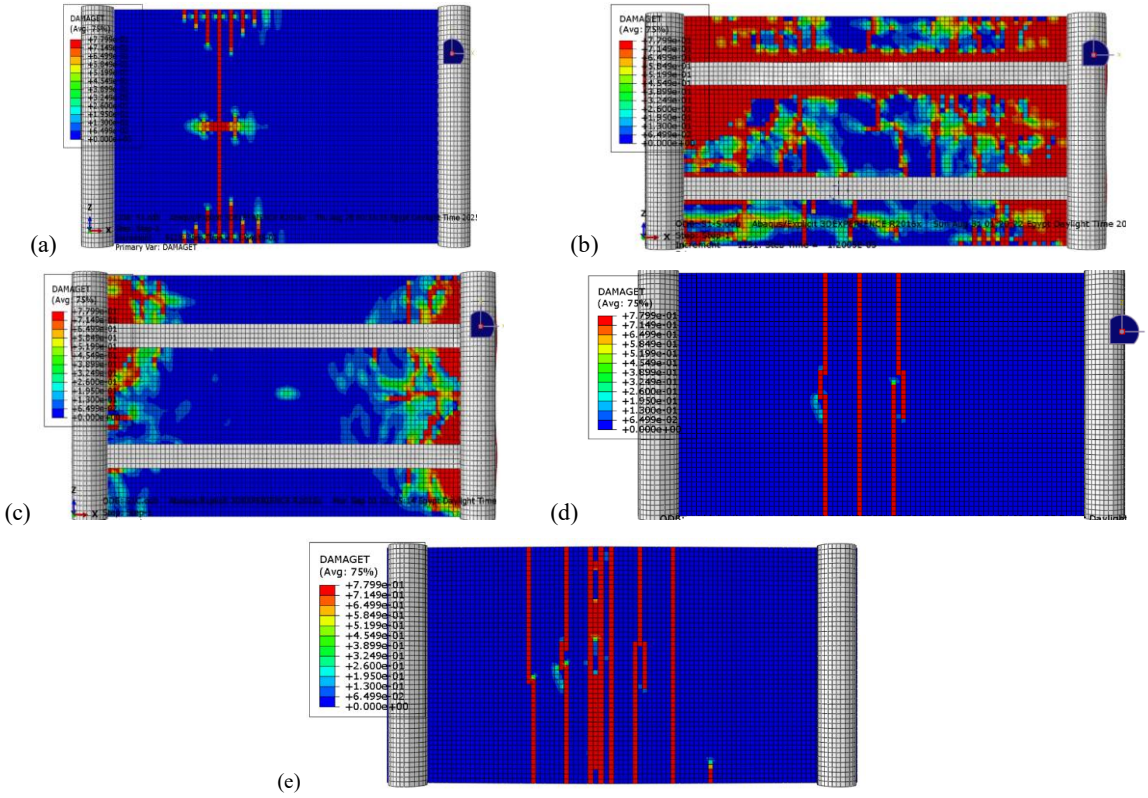

Figure 19. FEM failure mode of Slabs in group 1; (a) S2, (b) S2-S, (c) S2-C, (d) S2-E, and (d) S2-EM

7. Conclusions

Based on the analysis of the experimental results of the tested RC beams in this work, the following conclusions can be drawn:

- Crack initiation and propagation: In control slabs (S1, S2), cracks initiated at ~44–46% of ultimate load, while strengthened slabs delayed initiation to ~45–57% depending on the technique. In CFRP-retrofitted slabs, cracks appeared at ~50% of failure load, whereas ECC and ECC and mesh retrofits also delayed cracking by promoting micro crack formation before coalescence.
- Ultimate load capacity: CFRP retrofitting achieved the highest strength gains (22% for S1 and 58.8% for S2), followed by ECC mesh (22–33%), and ECC mortar alone with moderate improvement. Steel plates, however, reduced ultimate strength by ~11–16% due to poor bonding.
- Failure modes: Un-strengthened slabs failed by flexural cracking; steel plate-retrofitted slabs failed by interfacial debonding; CFRP slabs failed by CFRP fracture/separation; ECC mortar slabs showed localized mid-span cracking; ECC mesh slabs exhibited mesh rupture after excessive loading.
- Load–deflection behavior: CFRP retrofitted slabs showed a distinct three-phase response (elastic, plateau, sudden drop). ECC-based retrofits improved ductility and allowed gradual post-peak response, while steel plates did not alter control behavior due to interface failure.
- Ductility performance: CFRP and ECC mesh improved ductility (up to 43% for S1-EM), while ECC alone also enhanced deformability. Steel plate retrofitting reduced ductility by 2–9%.
- Energy absorption: CFRP and ECC mesh substantially increased energy dissipation (up to ~97% improvement), while steel plates decreased absorption capacity by ~34–36%.
- Stress distribution and resilience: ECC mortar improved stress redistribution and delayed crack localization; combining ECC with mesh provided additional confinement and resilience under flexural loading.
- Experimental–numerical correlation: FEM models accurately reproduced crack initiation, propagation, failure modes, and load–deflection responses, with an average FEM-to-test ultimate load ratio of 1.04 (SD = 0.027), confirming reliability of the numerical approach.

7.1. Hypothesis Statement

Based on the theoretical principles of composite action, bond behavior, and material constitutive characteristics, it was hypothesized that the performance of retrofitted RC slabs would vary significantly depending on the strengthening technique. Specifically, CFRP retrofitting was expected to provide the highest enhancement in ultimate load capacity due to its superior tensile strength and stiffness, albeit with a more brittle failure response. In contrast, engineered cementitious composites (ECC), owing to their strain-hardening and multiple micro cracking behavior, were anticipated to delay crack initiation, improve ductility, and enhance energy absorption through distributed cracking and stress redistribution. The integration of ECC with steel or polymer mesh was expected to further strengthen crack control and post-peak resilience by providing confinement and preventing crack coalescence. Conversely, slabs strengthened with externally bonded steel plates were hypothesized to show limited improvement or potential reduction in capacity due to interfacial debonding and incompatibility of stiffness between the plate and the concrete substrate. These theoretical expectations guided the experimental and numerical investigations and were subsequently confirmed by the observed improvements in cracking behavior, load capacity, ductility, and energy absorption in the strengthened slabs.

8. Declarations

8.1. Author Contributions

Conceptualization, F.M.E. and A.E.S.; methodology, A.E.S. and I.A.M.; software, I.A.M.; validation, F.M.E., A.E.S., and I.A.M.; formal analysis, I.A.M.; investigation, A.E.S.; resources, A.E.S.; data curation, I.A.M.; writing—original draft preparation, I.A.M.; writing—review and editing, A.E.S.; visualization, I.A.M.; supervision, F.M.E.; project administration, A.E.S. All authors have read and agreed to the published version of the manuscript.

8.2. Data Availability Statement

The data are not publicly available due to ongoing related research.

8.3. Funding

The authors received no financial support for the research, authorship, and/or publication of this article.

8.4. Acknowledgments

The authors would like to acknowledge the support of the Structural Engineering Laboratory staff at the Faculty of Engineering for their assistance during the experimental testing phase. The authors also appreciate the constructive discussions that contributed to improving the quality of this work.

8.5. Conflicts of Interest

The authors declare no conflict of interest.

9. References

[1] Hawileh, R. A., Nawaz, W., Abdalla, J. A., & Saqan, E. I. (2015). Effect of flexural CFRP sheets on shear resistance of reinforced concrete beams. Composite Structures, 122, 468–476. doi:10.1016/j.compstruct.2014.12.010.

[2] Boyd, A. J., Banthia, N., & Mindess, S. (2009). Retrofit of shear strength deficient RC beams with sprayed GFRP. Brittle Matrix Composites 9, 1–10. doi:10.1533/9781845697754.1.

[3] Tsonos, A. G. (2008). Effectiveness of CFRP-jackets and RC-jackets in post-earthquake and pre-earthquake retrofitting of beam-column subassemblages. Engineering Structures, 30(3), 777–793. doi:10.1016/j.engstruct.2007.05.008.

[4] Ha, G. J., Kim, Y. Y., & Cho, C. G. (2008). Groove and embedding techniques using CFRP trapezoidal bars for strengthening of concrete structures. Engineering Structures, 30(4), 1067–1078. doi:10.1016/j.engstruct.2007.07.006.

[5] Varma, A. H., Ricles, J. M., Sause, R., & Lu, L.-W. (2002). Experimental Behavior of High Strength Square Concrete-Filled Steel Tube Beam-Columns. Journal of Structural Engineering, 128(3), 309–318. doi:10.1061/(asce)0733-9445(2002)128:3(309).

[6] Hueste, M. B. D., & Bai, J. W. (2007). Seismic retrofit of a reinforced concrete flat-slab structure: Part I - seismic performance evaluation. Engineering Structures, 29(6), 1165–1177. doi:10.1016/j.engstruct.2006.07.023.

[7] Reyes, J. C., Rincon, R., Yamin, L. E., Correal, J. F., Martinez, J. G., Sandoval, J. D., Gonzalez, C. D., & Angel, C. C. (2020). Seismic retrofitting of existing earthen structures using steel plates. Construction and Building Materials, 230. doi:10.1016/j.conbuildmat.2019.117039.

[8] Bonacci, J. F., & Maalej, M. (2000). Externally Bonded FRP for Service-Life Extension of RC Infrastructure. Journal of Infrastructure Systems, 6(1), 41–51. doi:10.1061/(asce)1076-0342(2000)6:1(41).

[9] Attia, M. M., Abdelsalam, B. A., Tobbala, D. E., & Rageh, B. O. (2023). Flexural behavior of strengthened concrete beams with multiple retrofitting systems. Case Studies in Construction Materials, 18. doi:10.1016/j.cscm.2023.e01862.

[10] Ganesh, P., & Murthy, A. R. (2019). Repair, retrofitting and rehabilitation techniques for strengthening of reinforced concrete beams - A review. Advances in Concrete Construction, 8(2), 101–117. doi:10.12989/ACC.2019.8.2.101.

[11] Silpa, S., & Joy, C. M. (2021). Seismic Retrofitting of Structures Using Steel Bracing: An Overview. Proceedings of International Web Conference in Civil Engineering for a Sustainable Planet, 253–261. doi:10.21467/proceedings.112.32.

[12] Olajumoke, A. M., & Dundu, M. (2014). Methods for flexural strengthening of reinforced concrete elements using steel plates. Construction Materials and Structures, IOP Press, Bristol, United Kingdom. doi:10.3233/978-1-61499-466-4-1080.

[13] Teng, J. G., Chen, J. F., Smith, S. T., & Lam, L. F. R. P. (2002). FRP: strengthened RC structures. Wiley, Hoboken, United States. doi:10.1002/pi.1312.

[14] Rusnak, C. R. (2025). Sustainable Strategies for Concrete Infrastructure Preservation: A Comprehensive Review and Perspective. Infrastructures, 10(4), 99. doi:10.3390/infrastructures10040099.

[15] Esfahani, M. R., Kianoush, M. R., & Tajari, A. R. (2007). Flexural behaviour of reinforced concrete beams strengthened by CFRP sheets. Engineering Structures, 29(10), 2428–2444. doi:10.1016/j.engstruct.2006.12.008.

[16] Todut, C., Dan, D., & Stoian, V. (2015). Numerical and experimental investigation on seismically damaged reinforced concrete wall panels retrofitted with FRP composites. Composite Structures, 119, 648–665. doi:10.1016/j.compstruct.2014.09.047.

[17] Alharty, S. E., Khalil, E. A., & Hadhod, H. M. (2023). Strengthening of Reinforced Concrete Slabs using Carbon Fiber Polymers. Journal of Engineering Sciences, 51(4), 242–254. doi:10.21608/jesaun.2023.189658.1202.

[18] Saeed, F. H., Hejazi, F., & Rashid, R. S. M. (2025). Mechanical anchorage system in retrofitting of RC slabs using CFRP rods and concrete jacket. Archives of Civil and Mechanical Engineering, 25(2), 72. doi:10.1007/s43452-025-01127-4.

[19] Alobaidi, H. E., & Al-Zuhairi, A. H. (2023). Structural Strengthening of Insufficiently Designed Reinforced Concrete T-Beams using CFRP Composites. Civil Engineering Journal, 9(8), 1880–1896. doi:10.28991/cej-2023-09-08-05.

[20] Yalcin, C., Kaya, O., & Sinangil, M. (2008). Seismic retrofitting of R/C columns having plain rebars using CFRP sheets for improved strength and ductility. Construction and Building Materials, 22(3), 295–307. doi:10.1016/j.conbuildmat.2006.08.017.

[21] Galal, K., Seif ElDin, H. M., & Tirca, L. (2012). Flexural Performance of Steel Girders Retrofitted Using CFRP Materials. Journal of Composites for Construction, 16(3), 265–276. doi:10.1061/(asce)cc.1943-5614.0000264.

[22] Lee, H. S., Shin, S. H., & Kyung, J. W. (2007). Effect of Carbon Fiber Sheets on Flexural Strengthening of RC Beams Damaged by Corrosion of Tension Rebar. Key Engineering Materials, 348–349, 437–440. doi:10.4028/www.scientific.net/kem.348-349.437.

[23] Haddad, R. H., & Harb, A. N. (2021). Varying Profiles of CFRP Ropes for Strengthening Concrete Beams. International Journal of Civil Engineering, 20(4), 405–419. doi:10.1007/s40999-021-00664-2.

[24] Chataigner, S., Benzarti, K., Foret, G., Caron, J. F., Gemignani, G., Brugiolo, M., Calderon, I., Piñero, I., Birtel, V., & Lehmann, F. (2018). Design and testing of an adhesively bonded CFRP strengthening system for steel structures. Engineering Structures, 177, 556–565. doi:10.1016/j.engstruct.2018.10.004.

[25] Yücel, H. E., Dutkiewicz, M., & Yıldızhan, F. (2022). Application of ECC as a Repair/Retrofit and Pavement/Bridge Deck Material for Sustainable Structures: A Review. Materials, 15(24), 8752. doi:10.3390/ma15248752.

[26] Shang, X., Yu, J., Li, L., & Lu, Z. (2019). Strengthening of RC Structures by Using Engineered Cementitious Composites: A Review. Sustainability, 11(12), 3384. doi:10.3390/su11123384.

[27] Kim, M. J., Chun, B., Choi, H. J., Shin, W., & Yoo, D. Y. (2021). Effects of supplementary cementitious materials and curing condition on mechanical properties of ultra-high-performance, strain-hardening cementitious composites. Applied Sciences (Switzerland), 11(5), 2394. doi:10.3390/app11052394.

[28] Arundhathy, S., & Vasugi, V. (2016). Engineered cementitious composites for sustainable construction. Key Engineering Materials, 692, 17–26. doi:10.4028/www.scientific.net/KEM.692.17.

[29] Hyun, J. H., Bang, J. W., Lee, B. Y., & Kim, Y. Y. (2021). Effects of the replacement length of concrete with ECC on the cyclic behavior of reinforced concrete columns. Materials, 14(13), 3542. doi:10.3390/ma14133542.

[30] Ma, H., Yi, C., & Wu, C. (2021). Review and outlook on durability of engineered cementitious composite (ECC). Construction and Building Materials, 287, 122719. doi:10.1016/j.conbuildmat.2021.122719.

[31] Li, V. C. (2003). On Engineered Cementitious Composites (ECC). Journal of Advanced Concrete Technology, 1(3), 215–230. doi:10.3151/jact.1.215.

[32] Hu, Z., Elchalakani, M., Yehia, S., Ran, H., Sadakkathulla, M. A., & Guo, X. (2024). Engineered cementitious composite (ECC) strengthening of reinforced concrete structures: A state-of-the-art review. Journal of Building Engineering, 86, 108941. doi:10.1016/j.jobe.2024.108941.

[33] Sagare, S. S., Kirthiga, R., & Elavenil, S. (2024). A state of art of review on strengthening of concrete structures using fabric reinforced cementitious matrix. Research on Engineering Structures and Materials, 10(3), 1231–1260. doi:10.17515/resm2024.133ma1226rv.

[34] ACI 318-19. (2022). Building code requirements for structural concrete and commentary. American Concrete Institute (ACI), Farmington Hills, United States.

[35] Mhalhal, J. M., Al-Gasham, T. S., & Abid, S. R. (2020). Tests on reinforced concrete deep beams with different web reinforcement types. IOP Conference Series: Materials Science and Engineering, 988(1), 12032. doi:10.1088/1757-899X/988/1/012032.

[36] Al-Gasham, T. S., Mhalhal, J. M., & Abid, S. R. (2020). Evaluating planner hoop steel plates as web reinforcement for deep reinforced concrete beams. IOP Conference Series: Materials Science and Engineering, 988(1), 12031. doi:10.1088/1757-899X/988/1/012031.

[37] Jabir, H. A., Mhalhal, J. M., Al-Gasham, T. S., & Abid, S. R. (2020). Mechanical characteristics of deep beams considering variable a/d ratios: An experimental investigation. IOP Conference Series: Materials Science and Engineering, 988(1), 12030. doi:10.1088/1757-899X/988/1/012030.

[38] ASTM C39/C39M-05. (2003). Standard Test Method for Compressive Strength of Cylindrical Concrete Specimens. ASTM International, Pennsylvania, United States. doi:10.1520/C0039_C0039M-05.

[39] Dassault Systèmes. (2016). Abaqus 2016 documentation. Dassault Systèmes, Vélizy-Villacoublay, France.

[40] Zhang, D., Wang, Q., & Dong, J. (2016). Simulation study on CFRP strengthened reinforced concrete beam under four-point bending. Computers and Concrete, 17(3), 407–421. doi:10.12989/cac.2016.17.3.407.

[41] Ibrahim, S. K., & Rad, M. M. (2020). Numerical Plastic Analysis of Non-Prismatic Reinforced Concrete Beams Strengthened by Carbon Fiber Reinforced Polymers. Proceedings of the 13th fib International Ph.D. Symposium in Civil Engineering, 26-28 August, Paris, France.

[42] Camanho, P. P. (2001). Numerical simulation of delamination growth in composite materials. NASA Langley Research Center, National Aeronautics and Space Administration (NASA), Washington, United States.

[43] Jin, L., Jiang, X., Lu, K., & Du, X. (2022). Tests on shear failure and size effect of CFRP-wrapped RC beams without stirrups: Influence of CFRP ratio. Composite Structures, 291, 115613. doi:10.1016/j.compstruct.2022.115613.

[44] Qazi, A. U., Rasool, A. M., Din Afzal, M. F. U., Hameed, A., Mahmood, N., & Yaseen, N. (2024). Strengthening and retrofitting of low strength reinforced concrete slabs with high strength overlay: experimental and numerical investigation. International Journal of Structural Engineering, 14(4), 416–436. doi:10.1504/IJSTRUCTE.2024.142108.

[45] Lattif, Y., & Hamdy, O. (2022). An experimental investigation of the flexural strengthening of preloaded self-compacted RC beams using CFRP sheets and laminates composites. Advances in Concrete Construction, 13(4), 307–313. doi:10.12989/acc.2022.13.4.307.

[46] Samarakoon, S. M. S. M. K., Piatek, B., & De Silva, G. H. M. J. S. (2023). Investigation of the Flexural Behavior of Preloaded and Pre-Cracked Reinforced Concrete Beams Strengthened with CFRP Plates. Materials, 16(1), 22. doi:10.3390/ma16010022.

[47] Abd Elmoaty, A. E. M., Morsy, A. M., & Harraz, A. B. (2022). Effect of Fiber Type and Volume Fraction on Fiber Reinforced Concrete and Engineered Cementitious Composite Mechanical Properties. Buildings, 12(12), 2108. doi:10.3390/buildings12122108.

[48] Breveglieri, M., & Czaderski, C. (2021). RC slabs strengthened with externally bonded CFRP strips under long-term environmental exposure and sustained loading. Part 2: Laboratory experiments. Composites Part C: Open Access, 6. doi:10.1016/j.jcomc.2021.100210.

[49] Yang, X., Wang, X. D., Lin, Z. H., & Peng, H. (2025). Corroded RC slabs retrofitted with FRP grid-reinforced ECC matrix composites. Advances in Structural Engineering, 28(13), 2538–2556. doi:10.1177/13694332251334828.

[50] Ahamed, M. K., Wang, H., Ameri, A., & Hazell, P. J. (2023). Nacre-inspired design of engineered cementitious composite (ECC) beams for enhanced impact resistance and energy absorption. Journal of Building Engineering, 78. doi:10.1016/j.jobe.2023.107687.